SCIENTIFIC REPORTS

OPEN

SUBJECT AREAS:
CATALYST SYNTHESIS
NANOPARTICLES

Received
28 April 2014

Accepted
3 July 2014

Published
21 July 2014

Correspondence and requests for materials should be addressed to L.M.R. (lrossi@iq.usp.br)

Volcano-like Behavior of Au-Pd Core-shell Nanoparticles in the Selective Oxidation of Alcohols

Tiago A. G. Silva[1], Erico Teixeira-Neto[1], Núria López[2] & Liane M. Rossi[1]

[1]Departamento de Química Fundamental, Instituto de Química, Universidade de São Paulo, Av. Prof. Lineu Prestes 748, São Paulo, 05508-000, SP (Brazil), [2]Institute of Chemical Research of Catalonia, ICIQ, Av. Països Catalans 16, 43007, Tarragona (Spain).

Gold-palladium (AuPd) nanoparticles have shown significantly enhanced activity relative to monometallic Au and Pd catalysts. Knowledge of composition and metal domain distributions is crucial to understanding activity and selectivity, but these parameters are difficult to ascertain in catalytic experiments that have primarily been devoted to equimolar nanoparticles. Here, we report AuPd nanoparticles of varying Au:Pd molar ratios that were prepared by a seed growth method. The selective oxidation of benzyl alcohol was used as a model reaction to study catalytic activity and selectivity changes that occurred after varying the composition of Pd in bimetallic catalysts. We observed a remarkable increase in catalytic conversion when using a 10 : 1 Au:Pd molar ratio. This composition corresponds to the amount of Pd necessary to cover the existing Au cores with a monolayer of Pd as a full-shell cluster. The key to increased catalytic activity derives from the balance between the number of active sites and the ease of product desorption. According to density functional theory calculations, both parameters are extremely sensitive to the Pd content resulting in the volcano-like activity observed.

Optimizing the architectures of bimetallic nanoparticles constitutes a major goal to merge synthesis with structure-activity relationships that allow the rational design of catalysts[1,2]. Gold-palladium nanoparticles (AuPd NPs) have shown significantly enhanced catalytic activity relative to monometallic Au and Pd NP catalysts in prototypical reactions, such as CO oxidation[3,4], and in industrially challenging reactions, such as vinyl acetate monomer (VAM) synthesis[5], the direct synthesis of hydrogen peroxide from H_2 and O_2[6], alkene epoxidation[7], and the oxidation of hydrocarbons[8] and alcohols[9,10]. Bimetallic nanoparticles are formed by metallic domain distributions ranging from homogeneous alloys (AB) to core-shell ($A_{core}@B_{shell}$ or $B_{core}@A_{shell}$) nanoparticles. The type of morphology prepared depends on the synthetic protocol, the miscibility of both metals, and post-synthesis treatment. Pd and Au are miscible in almost all compositions, forming AuPd alloy NPs[5,11–14]. The AuPd alloy NPs most frequently used in catalytic applications contain a 1 : 1 Au:Pd molar ratio. However, it has been well documented that the surface of a AuPd alloy NP differs from its corresponding bulk concentration[15,16]. Enache et al.[9] have shown that Pd segregates towards the surface upon calcination, producing alloy NPs with a Pd-rich shell and an Au-rich core. Therefore, the active catalyst has a surface that is significantly enriched with Pd, obtained by the metal's migration to the surface during the annealing process. Additionally, core-shell NPs can be produced by the reduction of Pd over preformed Au NPs, and vice versa. Henning et al[10] have shown the preparation of core-shell Au-Pd catalysts by the growth of Pd on icosahedral Au seeds through thermodynamic control. In catalytic studies, they identified a 12 atomic-layer-thick Pd shell (2.2 nm) as the optimum catalyst for benzyl alcohol oxidation. However, no mechanistic explanation was given for the observed composition effects. NPs with different Au:Pd molar ratios have also been suggested as the most active catalysts in other studies[8,17–21]. Thus, the question of which is the best Au:Pd ratio in the optimal catalyst for a given reaction and why, still remains unanswered. Here we synthesized $Au_{core}@Pd_{shell}$ NPs with low Pd loading and investigated how the catalytic activity and selectivity were affected both experimentally and theoretically.

Results and Discussion

The preparation of bimetallic Au@Pd nanoparticles was based on the reduction of varying amounts of palladium over supported gold nanoparticles (Au NPs). The catalyst support chosen for this study is comprised of magnetic cores ($Fe_3O_4 \sim 10$ nm) spherically coated with silica (spheres of ~40 nm in diameter)[22]. The catalyst support was loaded with Au^{3+} ions (0.9 wt%, determined by ICP OES), and supported Au NPs were formed by controlled

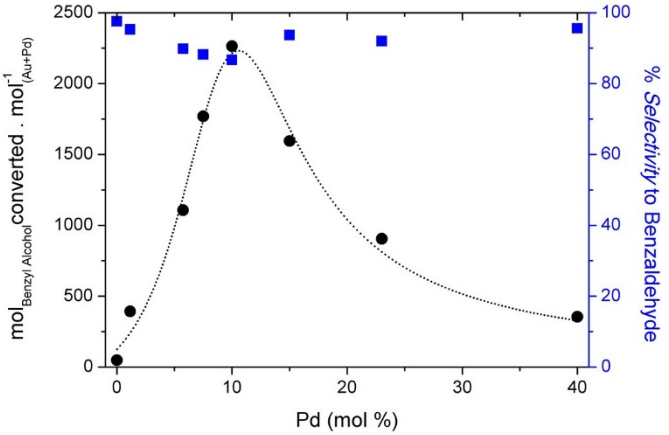

Figure 1 | Catalytic performance of the Au@Pd core-shell NP catalysts in the oxidation of benzyl alcohol. The amount of Au is fixed (3.4 μmol), while the amount of Pd varies from 0 to 40 mol % (i.e., 0 to 1.4 μmol).

reduction in molecular hydrogen. The morphology and size of the Au NPs used as seeds for the deposition of Pd were determined using a scanning transmission electron microscope (STEM). The Au NPs demonstrated a mean diameter of 12.0 ± 3.2 nm, according to representative High Angle Annular Dark Field (HAADF)-STEM images and the size distribution histogram fitted to a Gaussian function shown in Figure S1. In a second step, Pd (II) acetate solutions in benzyl alcohol containing variable amounts of Pd^{2+} ions were added over the Au cores and the reduction of Pd occurred in molecular hydrogen for 30 minutes at 100°C and 4 bar H_2. The amount of Au (in mols) in the resultant Au@Pd NPs remained fixed, while the Pd composition varied from 1 to 40 mol % relative to Au, corresponding to 0 to 4 monolayers (ML) of Pd. The aerobic oxidation of benzyl alcohol was used as a model reaction to study the activity and selectivity of the Au@Pd core-shell NP catalysts (Figure 1). Conversion of benzyl alcohol and selectivity obtained by selected Au@Pd core-shell NP catalysts and monometallic Au and Pd NP catalysts are presented in Table 1. The monometallic Au catalyst promoted high selectivity for benzaldehyde formation, but less than 2% conversion (Table 1 entry 1). Both conversion and selectivity were poor for the monometallic Pd catalyst prepared by adding the corresponding amount of Pd to the support without gold (Table 1 entry 9). The bimetallic catalysts exhibited a strong dependence between the activity and the amount of palladium added as shell metal. The highest benzyl alcohol conversion was achieved by adding 10 mol % Pd in respect to the existing amount of Au (i.e., Au:Pd = 10 : 1) (Table 1, entry 5). A sharp increase in benzyl alcohol conversion was observed by adding

Table 1 | Catalytic oxidation of benzyl alcohol by Au, Pd and Au@Pd catalysts

	Catalyst			Selectivity (%)			
Entry	μmol Au	μmol Pd	Conv. (%)	I	II	III	IV
1	3.4	0	1.7	-	97.6	0	2.4
2	3.4	0.039	14.0	-	95.2	1.7	3.0
3	3.4	0.20	41.2	-	89.8	7.6	2.6
4	3.4	0.26	67.0	0.2	88.2	7.8	3.7
5	3.4	0.34	87.7	0.4	86.4	9.4	3.9
6	3.4	0.51	64.6	0.3	93.3	3.0	3.3
7	3.4	0.78	39.2	0.3	91.8	4.3	3.6
8	3.4	1.4	17.5	0.6	95.0	1.9	2.5
9	0	3.4	10.0	26.7	67.8	2.5	3.1
10	0	6.8	30.2	2.3	89.7	4.1	3.9

I-Toluene; II-Benzaldehyde; III- Benzoic acid; IV-Benzyl benzoate. Reaction conditions: benzyl alcohol (9.6 mmol), T = 100°C, pO_2 = 6 bar, 2.5 h reaction.

Table 2 | Catalytic oxidation of benzyl alcohol by recycling Au@Pd (Au:Pd 10 : 1) catalyst

		Selectivity (%)			
Recycle	Conv. (%)	I	II	III	IV
1	60.1	0.2	93.7	4.5	1.6
2	56.3	0.3	96.3	2.1	1.3
3	65.1	4.2	94.3	0.9	0.5
4	37.7	2.7	93.8	2.4	1.1
5	45.2	2.2	93.7	3.1	1.0
6	50.3	2.0	92.5	4.6	0.9

I-Toluene; II-Benzaldehyde; III- Benzoic acid; IV-Benzyl benzoate. Reaction conditions: benzyl alcohol (9.6 mmol), bimetallic catalyst (3.4 μmol Au + 0.34 μmolPd), T = 100°C, pO_2 = 6 bar, 2.5 h reaction.

up to 10 mol % Pd (or 1 ML Pd), which was followed by a decrease as the Pd content was increased, as shown in Figure 1. The selectivity to benzaldehyde was only slightly affected by the Pd content of Au@Pd catalysts. After each reaction, the catalysts were easily separated by placing a magnet on the external reactor wall due to the magnetic properties of the catalyst support. The most active catalyst (Au:Pd = 10 : 1) was recycled and reused in successive reactions, maintaining the high selectivity to benzaldehyde (Table 2). Fluctuation in the reaction conversion was reported before for an alloyed AuPd catalyst[23] and can be related to the presence of amino-groups on the catalysts support (used to improve the impregnation of gold on the support[24]) and possible interactions between those groups and the reaction products.

The metal composition of the most active catalyst was determined by Flame Atomic Absorption Spectrometry (FAAS) to consist of mole fraction percentages of 89.9% Au and 9.1% Pd (i.e., Au:Pd = 10 : 1), which agrees with the nominal composition. This was also the case for other catalysts, as shown in Table 3, which suggests deposition of the desired amount of palladium.

The most active catalyst was also investigated by X-ray energy dispersive spectroscopy in a scanning transmission electron microscope (XEDS-STEM) to determine both the compositional distribution between particles and the existence of compositional rich domains within each particle. The mean composition (mole fraction) of the catalyst particles was determined to be 10.2 ± 6.7% Pd (see ESI for the details, Figure S2). The distribution of the metallic components within each particle was investigated using X-ray energy dispersive spectroscopy spectrum imaging (XEDS-SI). The XEDS-SI technique enables direct visualization of the nanoscale structural and compositional features of the synthesized core-shell particles[25]. Figure 2 shows a HAADF-STEM image of a quasi-spherical catalyst particle with the respective Au and Pd maps. In the compositional maps, the bright intensity in each pixel is a measurement of the number of X-ray peak counts at each corresponding position. Although the number of X-ray counts for Au Lα is larger than for Pd Lα in the investigated material (Figure S2), the brightness distribution was normalized in the maps shown in Figure 2. In the Au map, X-ray counts are measured throughout the particle, resulting in a hemisphere-shaped line scan. A different situation is observed in the Pd distribution because the number of counts increases steeply at the borders of the particle and remains nearly constant throughout the remainder of the particle. This distribution shows that the particles investigated are morphologically structured with an Au-rich core and a Pd-rich shell[12]. The less active catalyst with Au:Pd = 10 : 4 is also morphologically structured with an Au-rich core and a Pd-rich shell (Figure S3). Monometallic nanoparticles were not found in the investigated samples.

In the catalytic studies, we observed a volcano-like behavior characterized by a steady increase in benzyl alcohol conversion as the quantity of added Pd (shell metal) was increased relative to Au (core

Table 3 | Composition of Au and Pd in selected $Au_{core}@Pd_{shell}$ catalysts determined by FAAS

Catalyst (Au:Pd molar ratio)	%Au	%Pd	Au (μmol g^{-1})	Pd (μmol g^{-1})	Au:Pd molar ratio
Au@Pd (10 : 1)	1.42	0.08	72	7.5	1 : 0.10
Au@Pd (10 : 1.5)	1.14	0.12	58	11	1 : 0.18
Au@Pd (10 : 3)	0.99	0.16	50	15	1 : 0.30
Au@Pd (10 : 4)	1.28	0.27	64	25	1 : 0.39

metal), with a consistent decrease in conversion for more than 10 mol % Pd. If the Pd atoms are primarily on the surface of Au, as observed in the morphological studies, the composition of the most active catalyst (89.9% Au and 9.1% Pd) correlates with the composition required for the complete coverage of Au cores (d = 12.0 ± 3.2 nm) with one atomic layer of Pd (see Table S1). A special behaviour related to the monolayer regime was reported previously for other alloys[26–28].

Theoretical simulations are fundamental to the understanding of the volcano-like behavior reported in Figure 1. Density functional theory-based investigations of AuPd systems have concentrated on the structure[29–32], oxygen activation[33], or VAM synthesis[29–32,34]. Here we modelled the reaction process on three representative surfaces with an ordered surface alloy (ML denotes the number of Pd monolayers grown on the Au seeds): $Au@Pd_3Au$, Au@Pd(1 ML) and Au@Pd(2 ML) (Figure 3); and Pd.

With these material models and the PBE functional[35], we inspected the paths leading to the formation of the aldehyde, considering the following elementary steps:

(1) Alcohol adsorption: $C_6H_5CH_2OH(g) + * \rightarrow C_6H_5CH_2OH*$
(2) Oxygen adsorption: $O_2(g) + 2* \rightarrow 2O*$
(3) First H transfer: $C_6H_5CH_2OH* + O* \rightarrow C_6H_5CH_2O* + OH*$
(4) Second H transfer: $C_6H_5CH_2O* + OH* \rightarrow C_6H_5CHO* + H_2O*$
(5) Water desorption: $H_2O* \rightarrow H_2O(g) + *$
(6) Aldehyde desorption: $C_6H_5CHO* \rightarrow C_6H_5CHO(g) + *$
(7) Unselective path: $C_6H_5CHO* + H_2O* \rightarrow C_6H_5CHOH* + OH*$

The reaction profile is presented in Figure 4 for the bimetallic systems only. The activation barriers, not shown in the figure, and all data for the Pd-only system, are presented in Table S2. Analysis of the results in Figure 4 leads to the conclusion that adsorption of the alcohol is difficult (endothermic by 0.45 eV) on $Au@Pd_3Au$, and thus the reaction cannot progress adequately in such structures because the number of molecules adsorbed on the surface is small. Increasing the amount of Pd on the surface improves adsorption rendering it exothermic (−0.31 eV) as observed for Au@Pd(1 ML). When additional Pd is present in the slab, the binding energy is very strong, −1.69 eV for Au@Pd(2 ML). The reaction has easily attainable energy barriers for all of the steps (see Table S2). Water desorption (step 5) is exothermic for systems with Pd shells up to one monolayer (−0.66 and −0.22 eV for $Au@Pd_3Au$ and Au@Pd(1 ML), respectively), and endothermic for NPs having higher Pd content. In the reaction mechanism, the OH intermediate is a short living species due to the difficulties found in its formation and the easiness at which the next reaction takes place. Therefore, the main path for the unselective process is the back transfer of one proton from water, i.e. step 7. The reduced energy barrier for water desorption guarantees the selectivity towards benzaldehyde because the barrier for this step is, in all cases, lower than H transfer from water to the aldehyde (Table S2). The final aldehyde product is easily desorbed from the $Au@Pd_3Au$ model, but its binding energy is large on Pd monolayers: 0.8 and 1.1 eV, for 1 and 2 ML, respectively. As for the activity, reactant adsorption (1.7 vs. 0.3 eV) and product desorption (1.1 vs. 0.8 eV) are far two strong on the two monolayer system compared to the single layer to ensure a rapid recycling of the clean surface.

The computational approach is in line with the mechanistic investigations in the literature. For instance, Enache et al.[9] found zero order for oxygen, which is in agreement with the ease of dissociation of oxygen reported in previous calculations[33]. In addition, the apparent activation energy reported was 0.47 eV. This value is similar to

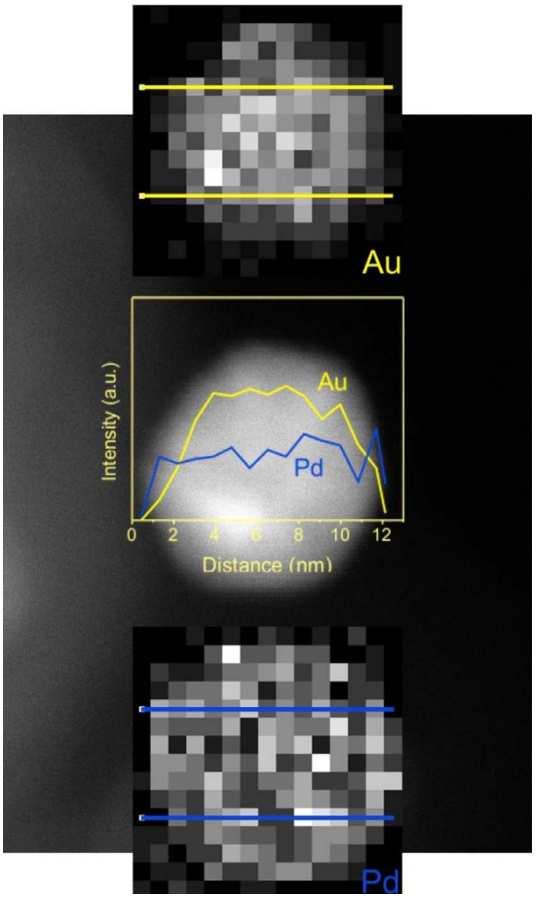

Figure 2 | HAADF-STEM image of a supported catalyst particle Au:Pd = 10 : 1 and the corresponding Au and Pd maps. The particle composition distribution is observed in the line scans, measured from the regions delimited by the lines indicated in both maps.

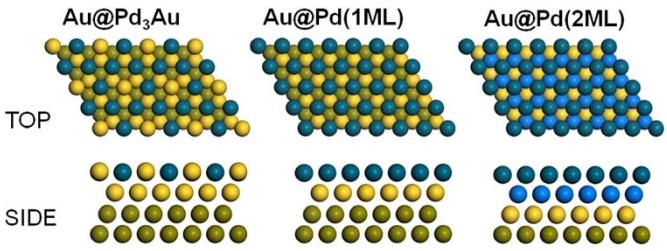

Figure 3 | The three model systems employed in the DFT calculations. Left a Pd_3Au overlayer on Au; center a Pd monolayer on Au and right two Pd monolayers on Au. Blue spheres stand for Pd atoms and yellow (olive) for Au.

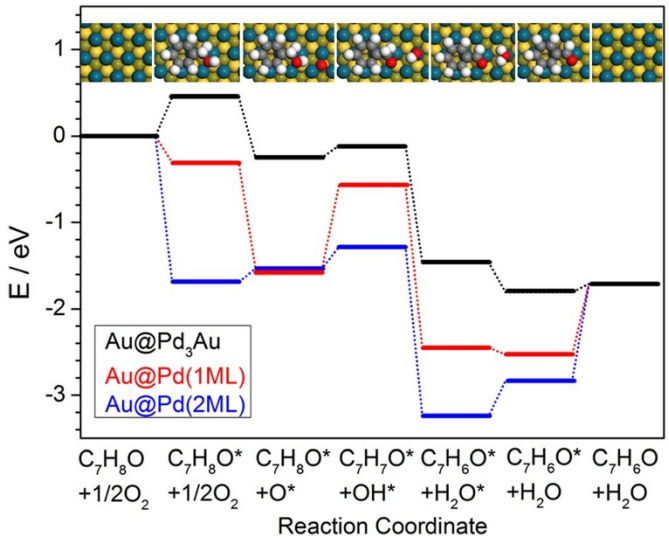

Figure 4 | Reaction profile for the selective oxidation of benzyl alcohol to the corresponding aldehyde. The insets schematically represent the different steps in the reaction for the Au@Pd(1 ML) model: blue spheres Pd, yellow Au, grey C, red O, white H (see also Figure S4).

the ΔG for the desorption of benzylaldehyde in Au@Pd(1 ML) once dispersion and entropic terms are considered (0.46 eV). Pd grown on Au has an upward shift of the Pd band by +0.30 eV[32]. Strain induced by Au on Pd should increase the reactivity as the Au lattice is larger than that of Pd. Indeed enhanced alcohol adsorption is found for the two Au@Pd(2 ML) model, −1.69 vs. −0.86 eV, see Table S2. However, the strong Pd-Au ligand effect is observed and indeed the ligand contribution affects alcohol adsorption to such an extension that the binding is −0.31 eV only. The calculations including entropy and dispersion were done as follows: $\Delta G = \Delta E - T\Delta S$; where S was only considered for the gas-phase species and ΔE included the dispersion terms calculated through the dispersion model introduced by Grimme et al.[36] and the metal parameters from Tkatchenko et al[37]. In the case of Pd, to analyze unselectivity, water desorption and unselective H transfer need to be considered. If entropic and dispersion contributions are considered desorption is endothermic by 0.3 eV while the barrier for proton transfer is as low as 0.14 eV, therefore selectivity is compromised.

The analysis of the reaction network accounts for the observation of a maximum in the experimental catalytic results. On the left side of the volcano-like plot (Figure 1) corresponding to low Pd loadings, DFT results indicate that adsorption of the alcohol is controlling the activity. The electronic properties of AuPd alloys have been extensively analyzed in the literature[29–32]. Actually, only sites with no Au would be active for benzyl alcohol adsorption, and thus, activity is proportional to the number of Pd ensembles (i.e., at least 6 Pd atoms on the surface) that can accommodate benzyl alcohol. However, increasing benzyl alcohol adsorption subsequently increases the desorption energy required to clean the surface from the aldehyde product. This is a drawback when having more than 1 ML of Pd, as the binding energy of the aldehyde is far too large to remove the product from the surface and leave clean ensembles for the next catalytic cycle. As a consequence, the best balance is obtained when 1 ML of Pd covers the Au nanoparticles because benzyl alcohol adsorption can then occur everywhere and desorption is still feasible. For the Pd-only system, the barrier for the second H transfer is the most energy-demanding step, 1.32 eV (Table S2), and thus implies that the reaction is slow at the temperatures at which AuPd alloys are active. In addition, once the aldehyde is formed, the water desorption energy and the barrier for H stripping are comparable (0.10 vs. 0.14 eV, respectively), and therefore, compromising selectivity determining step is not as favorable as for the alloys. When extending the study to other unsaturated alcohols the selectivity controlled by the competition between steps (5) and (7) would follow the same general rule. As for the activity, the adsorption of these unsaturated alcohols (like crotyl alcohol) needs smaller ensembles than those of the corresponding benzyl alcohol, but again the number of sites would maximize for a composition of 1 ML of Pd on top of the Au core. Therefore, the present results can be extrapolated to other unsaturated alcohols.

Conclusions

We have shown that the rational design based on the density functional theory and the controlled synthesis of Au@Pd core-shell catalysts with specific compositions and metal domain distributions can be used as a strategy to enhance the catalytic properties of Au while maintaining its high selectivity for the oxidation of benzyl alcohol to benzaldehyde. This finding shows that many opportunities remain to obtain enhanced properties in bimetallic nanomaterials by tailoring the amount of each metal and the metal domain distribution, and opens new possibilities in the field of nanomaterials synthesis and design.

Methods

Synthesis of the catalyst support. The core-shell Fe_3O_4@SiO_2 nanocomposite was prepared and modified with (3-aminopropyl)triethoxysilane as reported in the literature[38].

Synthesis of the supported Au monometallic catalyst. The catalyst support, silica-coated magnetite nanoparticles previously modified with (3-aminopropyl)triethoxysilane (500 mg), was added to an aqueous solution of $HAuCl_4$ (40 mL, 0.215 g L^{-1}) with pH 6. The mixture was stirred at 25°C for 2 h. The solid was then collected magnetically from the solution and washed twice with hot distilled water and twice with ethanol. The reduction step was performed in a Fischer–Porter glass reactor pressurized with hydrogen gas. The gold precursor was dispersed in cyclohexane and heated to 100°C under H_2 at 4 bar. The mixture was stirred for 2 h, and the color of the solid changed from brown to dark red.

Synthesis of the supported AuPd bimetallic catalysts. The preparation of bimetallic catalysts consisted of an addition of the desired amount of a $Pd(OAc)_2$ solution in benzyl alcohol (20 to 800 μL, $[Pd^{2+}] = 1.68 \times 10^{-3}$ mol L^{-1}) to 75 mg of Au monometallic catalyst (3.4 μmol Au), which was then added to a Fischer–Porter 100 mL glass reactor. Benzyl alcohol was added to achieve a total volume of 1.0 mL and the reactor was pressurized with hydrogen gas at 4 bar. The mixture was stirred for 30 min at 100°C. The color of the solid changed to black. The reactor was cooled to room temperature, the hydrogen gas was relieved, and the reaction mixture was kept inside the reactor for catalytic studies.

Catalytic experiments. All reactions were performed using a modified Fischer–Porter 100 mL glass reactor. In a typical reaction, the glass reactor was loaded with the supported Au catalyst (75 mg, 3.4 μmol Au) and benzyl alcohol (9.6 mmol), or the bimetallic Au-Pd catalyst-containing mixture was prepared as described above. The reactor was purged three times with O_2, leaving the vessel at 6 bar. The temperature was maintained at 100°C with an oil bath on a hot stirring plate connected to a digital controller (ETS-D5 IKA). The reactions were constantly stirred using Teflon-coated magnetic stir bars for the desired amount of time. The catalyst was recovered magnetically by affixing a magnet onto the reactor wall. The products were collected with a syringe and analyzed by gas chromatography (GC) and gas chromatography-mass spectrometry (GC-MS).

Morphological investigation. Catalyst samples were prepared by sonicating the catalyst powder in isopropanol. A drop of the resulting dispersion was placed on a thin carbon film, which was deposited on standard 400-mesh TEM copper grids and air-dried. The size distribution of the supported Au core particles was investigated by HAADF-STEM using a JEOL-JEM 2100F TEM microscope available at the LNNano Laboratory (CNPEM, Campinas, Brazil). The mean diameter distribution was measured by HAADF image analysis using Image-Pro Plus 6.0 software. Two hundred nanoparticles were measured to build the size distribution histogram that is presented. Compositional distribution was measured on the same instrument by acquiring individual XEDS-STEM spectra of a sample of 62 supported particles. Particle compositional maps were acquired by XED-Spectrum Imaging with a Digital Micrograph 1.8 system (Gatan Inc.) controlling a Thermo-Noran XEDS. The SIs were acquired at a 15 × 15 pixel resolution with a dwell time of 2 s/pixel, using the drift correction facility every 100 s. XED spectra were acquired in the 0–10 keV energy range at each pixel. Electron probe sizes of approximately 0.7 nm were obtained by operating the JEM 2100F instrument in STEM mode, allowing enough current

density at each sample point to acquire statistically significant X-ray counts for the investigated elements.

Computational Methods. Density Functional Theory was applied to slabs modeling the system. The VASP program was employed to this end[39,40]. The functional of choice was PBE[35]. Inner electrons were replaced by frozen cores PAW[41] and valence electrons were expanded in plane waves with cut-off energy of 450 eV. As the particles are large enough only (111) surfaces, the most stable for fcc metals, have been employed in the simulations. Three different models were employed to represent the surface of the Pd grown on Au particles: the first one is a partial monolayer on the surface of Au@Pd_3Au composition, this is following one of the ordered alloys, a single Pd monolayer on Au, and a Pd bilayer on Au (see Fig. 3) and Pd alone. The slabs contain four layers of metal in total and in all cases overlayers follow the lattice parameter of Au. The vacuum space interleaving the slabs is at 15 Å. As the adsorbates are large we have employed a surface reconstructions $p(6 \times 4)$ that can account for the adsorption of the benzyl alcohol and its derivates. On these supercells the k-point sampling employed are $2 \times 5 \times 1$ Monkhorst-Pack points centered at gamma point[42]. Transition state searches were performed with the climbing image version of the Nudged Elastic Band method[43].

1. Strasser, P. *et al.* Lattice-strain control of the activity in dealloyed core–shell fuel cell catalysts. *Nat. Chem.* **2**, 454–460 (2010).
2. Serpell, C. J., Cookson, J., Ozkaya, D. & Beer, P. D. Core@shell bimetallic nanoparticle synthesis via anion coordination. *Nat. Chem.* **3**, 478–483 (2011).
3. Maroun, F., Ozanam, F., Magnussen, O. M. & Behm, R. J. The role of atomic ensembles in the reactivity of bimetallic electrocatalysts. *Science* **293**, 1811–1814 (2001).
4. Xu, J. *et al.* Biphasic Pd-Au alloy catalyst for low-temperature CO oxidation. *J. Am. Chem. Soc.* **132**, 10398–10406 (2010).
5. Chen, M., Kumar, D., Yi, C.-W. & Goodman, D. W. The promotional effect of gold in catalysis by palladium-gold. *Science* **310**, 291–293 (2005).
6. Landon, P., Collier, P. J., Papworth, A. J., Kiely, C. J. & Hutchings, G. J. Direct formation of hydrogen peroxide from H_2/O_2 using a gold catalyst. *Chem. Commun.* 2058–2059 (2002).
7. Hughes, M. D. *et al.* Tunable gold catalysts for selective hydrocarbon oxidation under mild conditions. *Nature* **437**, 1132–1135 (2005).
8. Kesavan, L. *et al.* Solvent-free oxidation of primary carbon-hydrogen bonds in toluene using Au-Pd alloy nanoparticles. *Science* **331**, 195–199 (2011).
9. Enache, D. I. *et al.* Solvent-free oxidation of primary alcohols to aldehydes using Au-Pd/TiO_2 catalysts. *Science* **311**, 362–365 (2006).
10. Henning, A. M. *et al.* Gold–palladium core–shell nanocrystals with size and shape control optimized for catalytic performance. *Angew. Chem., Int. Ed.* **52**, 1477–1480 (2013).
11. Lopez-Sanchez, J. A. *et al.* Reactivity studies of Au–Pd supported nanoparticles for catalytic applications. *Appl. Catal. A* **391**, 400–406 (2011).
12. Hagelin-Weaver, H. A. E., Weaver, J. F., Hoflund, G. B. & Salaita, G. N. Electron energy loss spectroscopic investigation of polycrystalline Au, Pd and a Pd–Au alloy. *J. Alloys Compd.* **393**, 93–99 (2005).
13. Hutchings, G. J. Nanocrystalline gold and gold palladium alloy catalysts for chemical synthesis. *Chem. Commun.* 1148–1164 (2008).
14. Robach, Y., Abel, M. & Porte, L. Initial stages of Pd deposition on $Au_{(1\,1\,0)}$: A STM, LEED and AES study. *Surf. Sci.* **526**, 248–256 (2003).
15. Wei, T., Wang, J. & Goodman, D. W. Characterization and chemical properties of Pd-Au alloy surfaces. **111**, 8781–8788 (2007).
16. Yi, C. W., Luo, K., Wei, T. & Goodman, D. W. The composition and structure of Pd-Au surfaces. *J. Phys. Chem. B* **109**, 18535–18540 (2005).
17. Villa, A., Wang, D., Su, D., Veith, G. M. & Prati, L. Using supported Au nanoparticles as starting material for preparing uniform Au/Pd bimetallic catalysts. *Phys. Chem. Chem. Phys.* **12**, 2183–2189 (2010).
18. Ishihara, T. *et al.* Synthesis of hydrogen peroxide by direct oxidation of H_2 with O_2 on Au/SiO_2 catalyst. *Appl. Catal., A* **291**, 215–221 (2005).
19. Pritchard, J. *et al.* Direct synthesis of hydrogen peroxide and benzyl alcohol oxidation using Au-Pd catalysts prepared by sol immobilization. *Langmuir* **26**, 16568–16577 (2010).
20. Marx, S. & Baiker, A. Beneficial interaction of gold and palladium in bimetallic catalysts for the selective oxidation of benzyl alcohol. *J. Phys. Chem. C* **113**, 6191–6201 (2009).
21. Alayoglu, S. *et al.* Surface composition and catalytic evolution of Au_xPd_{1-x} (x = 0.25, 0.50 and 0.75) nanoparticles under CO/O_2 reaction in torr pressure regime and at 200°C. *Catal. Lett.* **141**, 633–640 (2011).
22. Oliveira, R. L., Kiyohara, P. K. & Rossi, L. M. High performance magnetic separation of gold nanoparticles for catalytic oxidation of alcohols. *Green Chem.* **12**, 144–149 (2010).
23. Silva, T. A. G., Landers, R. & Rossi, L. M. Magnetically recoverable AuPd nanoparticles prepared by a coordination capture method as a reusable catalyst for green oxidation of benzyl alcohol. *Catal. Sci. Technol.* **3**, 2993–2999 (2013).
24. Oliveira, R. L., Zanchet, D., Kiyohara, P. K. & Rossi, L. M. On the stabilization of gold nanoparticles over silica-based magnetic supports modified with organosilanes. *Chem. Eur. J.* **17**, 4626–4631 (2011).
25. Wang, C. *et al.* Multimetallic Au/$FePt_3$ nanoparticles as highly durable electrocatalyst. *Nano Lett.* **11**, 919–926 (2010).
26. Schlapka, A., Lischka, M., Gross, A., Kasberger, U. & Jakob, P. Surface strain versus substrate interaction in heteroepitaxial metal layers: Pt on Ru(0001). *Phys. Rev. Lett.* **91**, 016101 (2003).
27. Alayoglu, S., Nilekar, A. U., Mavrikakis, M. & Eichhorn, B. Ru-Pt core-shell nanoparticles for preferential oxidation of carbon monoxide in hydrogen. *Nat. Mater.* **7**, 333–338 (2008).
28. Nilekar, A. U., Alayoglu, S., Eichhorn, B. & Mavrikakis, M. Preferential CO oxidation in hydrogen: reactivity of core-shell nanoparticles. *J. Am. Chem. Soc.* **132**, 7418–7428 (2010).
29. Soto-Verdugo, V. & Metiu, H. Segregation at the surface of an Au/Pd alloy exposed to CO. *Surf. Sci.* **601**, 5332–5339 (2007).
30. Boscoboinik, J. A., Plaisance, C., Neurock, M. & Tysoe, W. T. Monte Carlo and density functional theory analysis of the distribution of gold and palladium atoms on Au/Pd(111) alloys. *Phys. Rev. B* **77**, 045422 (2008).
31. Calaza, F., Stacchiola, D., Neurock, M. & Tysoe, W. T. Coverage effects on the palladium-catalyzed synthesis of vinyl acetate: comparison between theory and experiment. *J. Am. Chem. Soc.* **132**, 2202–2207 (2010).
32. Garcia-Mota, M. & Lopez, N. Temperature and pressure effects in CO titration of ensembles in PdAu(111) alloys using first principles. *Phys. Rev. B* **82**, 075411 (2010).
33. Garcia-Mota, M. & Lopez, N. The role of long-lived oxygen precursors on AuM alloys (M = Ni, Pd, Pt) in CO oxidation. *Phys. Chem. Chem. Phys.* **13**, 5790–5797 (2011).
34. Garcia-Mota, M. & Lopez, N. Template effects in vinyl acetate synthesis on PdAu surface alloys: a density functional theory study. *J. Am. Chem. Soc.* **130**, 14406–14407 (2008).
35. Perdew, J. P., Burke, K. & Ernzerhof, M. Generalized gradient approximation made simple. *Phys. Rev. Lett.* **77**, 3865–3868 (1996).
36. Grimme, S., Antony, J., Ehrlich, S. & Krieg, H. A consistent and accurate ab initio parametrization of density functional dispersion correction (DFT-D) for the 94 elements H-Pu. *J. Chem. Phys.* **132**, 154104 (2010).
37. Ruiz, V. G., Liu, W., Zojer, E., Scheffler, M. & Tkatchenko, A. Density-functional theory with screened van der waals interactions for the modeling of hybrid inorganic-organic systems. *Phys. Rev. Lett.* **108**, 146103 (2012).
38. Jacinto, M. J., Kiyohara, P. K., Masunaga, S. H., Jardim, R. F. & Rossi, L. M. Recoverable rhodium nanoparticles: synthesis, characterization and catalytic performance in hydrogenation reactions. *Appl. Catal., A* **338**, 52–57 (2008).
39. Kresse, G. & Furthmuller, J. Efficiency of ab-initio total energy calculations for metals and semiconductors using a plane-wave basis set. *Comput. Mater. Sci.* **6**, 15–50 (1996).
40. Kresse, G. & Furthmüller, J. Efficient iterative schemes for ab initio total-energy calculations using a plane-wave basis set. *Phys. Rev. B* **54**, 11169–11186 (1996).
41. Blochl, P. E. Projector augmented-wave method. *Phys. Rev. B* **50**, 17953–17979 (1994).
42. Monkhorst, H. J. & Pack, J. D. Special points for Brillouin-zone integrations. *Phys. Rev. B* **13**, 5188–5192 (1976).
43. Henkelman, G., Uberuaga, B. P. & Jonsson, H. A climbing image nudged elastic band method for finding saddle points and minimum energy paths. *J. Chem. Phys.* **113**, 9901–9904 (2000).

Acknowledgments

The authors acknowledge support from FAPESP, CNPq and INCT-Catalise. We also thank LNNano-CNPEM (Campinas, Brazil) for the use of TEM facilities. N.L. would like to thank ERC-2010-StG-258406, MINECO 2012-33826/BQU and BSC-RES for generously providing computational resources.

Author contributions

T.A.G.S. prepared and tested catalysts under the supervision of L.M.R. TEM measurements were carried out by E.T.N. and N.L. conducted DFT calculations. All authors contributed to the analysis of the data and the writing of the manuscript.

Additional information

Supplementary information accompanies this paper at http://www.nature.com/scientificreports

Competing financial interests: The authors declare no competing financial interests.

How to cite this article: Silva, T.A.G., Teixeira-Neto, E., López, N. & Rossi, L.M. Volcano-like Behavior of Au-Pd Core-shell Nanoparticles in the Selective Oxidation of Alcohols. *Sci. Rep.* **4**, 5766; DOI:10.1038/srep05766 (2014).